

DETERMINING THE HUBBLE CONSTANT FROM GRAVITATIONAL WAVE OBSERVATIONS OF MERGING COMPACT BINARIES

SAMAYA NISSANKE¹, DANIEL E. HOLZ², NEAL DALAL³, SCOTT A. HUGHES^{4,5,6},
 JONATHAN L. SIEVERS^{7,8}, CHRISTOPHER M. HIRATA¹

Draft version July 11, 2013

ABSTRACT

Recent observations have accumulated compelling evidence that some short gamma-ray bursts (SGRBs) are associated with the mergers of neutron star (NS) binaries. This would indicate that the SGRB event is associated with a gravitational-wave (GW) signal corresponding to the final inspiral of the compact binary. In addition, the radioactive decay of elements produced in NS binary mergers may result in transients visible in the optical and infrared with peak luminosities on hours-days timescales. Simultaneous observations of the inspiral GWs and signatures in the electromagnetic band may allow us to directly and independently determine both the luminosity distance and redshift to a binary. These standard sirens (the GW analog of standard candles) have the potential to provide an accurate measurement of the low-redshift Hubble flow. In addition, these systems are absolutely calibrated by general relativity, and therefore do not experience the same set of astrophysical systematics found in traditional standard candles, nor do the measurements rely on a distance ladder. We show that 15 observable GW and EM events should allow the Hubble constant to be measured with 5% precision using a network of detectors that includes advanced LIGO and Virgo. Measuring 30 beamed GW-SGRB events could constrain H_0 to better than 1%. When comparing to standard Gaussian likelihood analysis, we find that each event's non-Gaussian posterior in H_0 helps reduce the overall measurement errors in H_0 for an ensemble of NS binary mergers.

Subject headings: cosmology: distance scale—cosmology: theory—gamma rays: bursts—gravitational waves

1. INTRODUCTION

Gravitational wave (GW) standard sirens are the GW analogs to traditional standard candles. They exemplify multi-messenger astronomy (see Bloom *et al.* 2009, Phinney 2009, Kulkarni & Kasliwal 2009), where the use of both electromagnetic (EM) and GW measurements results in astrophysical insights inaccessible to either method alone. As originally discussed by Schutz (1986), inspiralling compact neutron star (NS) or black hole (BH) binaries are excellent standard sirens, in that their GW measurements could determine the sources' absolute distances. The only calibration (so to speak) in this measurement is the assumption that general relativity describes the binary waveform. When used in conjunction with a redshift measurement inferred by an independently observed EM counterpart, standard siren observations allow us to study the luminosity distance-redshift relationship. Consequently we may map out the

Universe's expansion history, and thereby constrain cosmological parameters such as the Hubble constant H_0 , the dark energy equation-of-state parameter w , and the average densities of matter Ω_m and dark energy Ω_Λ .

In this work we are interested in the constraints on the Hubble constant that result from observations of GW-EM standard sirens at low redshift ($z < 0.3$), as would be expected from the coming generation of ground-based GW observatories. This will complement existing H_0 measurements at the few percent level, which have been determined using a combination of methods; see Suyu *et al.* (2012) for a brief review and references therein. All methods aim to i) provide independent H_0 measurements, compared to derived constraints in the case of the Cosmic Microwave Background (CMB) and Baryon Acoustic Oscillations (BAO) measurements (see, for example, discussion of cosmological parameter constraints by the Planck Collaboration *et al.* 2013), and ii) reach a $\sim 1\%$ precision in random errors in the near future. For instance, the Planck satellite recently reported H_0 of $67.4 \pm 1.4 \text{ km s}^{-1} \text{ Mpc}^{-1}$, a low value compared to cosmic distance ladder results of $73.8 \pm 2.4 \text{ km s}^{-1} \text{ Mpc}^{-1}$ (HST Cepheid-SNIa; Riess *et al.* 2011a, Riess *et al.* 2011b) and 74.3 ± 1.5 [statistical] ± 2.1 [systematic] $\text{km s}^{-1} \text{ Mpc}^{-1}$ (Spitzer CHP; Freedman *et al.* 2012). Although the discrepancy between the CMB and cosmic distance ladder measures lies only at a $\sim 2.5 \sigma$ discrepancy, such differences suggest the necessity of additional independent measures. An independent $\sim 1\%$ measurement in H_0 is especially desirable when improving figure-of-merit constraints on the dark energy equation of state (Hu 2005; Weinberg *et al.* 2012). The control of systematics

¹ Caltech, Theoretical Astrophysics, California Institute of Technology, Pasadena, California 91125, USA

² Enrico Fermi Institute, Department of Physics, and Kavli Institute for Cosmological Physics, University of Chicago, Chicago, IL 60637, USA

³ Department of Astronomy, University of Illinois, 1002 W. Green St., Urbana, IL 61801, USA

⁴ Department of Physics and MIT Kavli Institute, MIT, 77 Massachusetts Ave., Cambridge, MA 02139, USA

⁵ Canadian Institute for Theoretical Astrophysics, University of Toronto, 60 St. George St., Toronto, ON M5S 3H8, Canada

⁶ Perimeter Institute for Theoretical Physics, Waterloo, ON N2L 2Y5, Canada

⁷ Jadwin Hall, Department of Physics, Princeton University, New Jersey, USA

⁸ Astrophysics and Cosmology Research Unit, University of Kwazulu-Natal, Westville, Durban, 4000, South Africa

is crucial in having a useful measurement of w , especially one that might involve the falsification of a cosmological constant as the origin of the dark energy. Standard siren approaches offer a fundamentally different set of systematics, and therefore provide a valuable counterpart to all other methods.

For the next generation of advanced ground based GW observatories, comprising LIGO⁹, Virgo¹⁰, and other GW interferometers, inspiralling and merging NS-NS and NS-BH binaries are expected to be the most numerous and characterizable events. For an advanced LIGO–Virgo network, predicted event rates for NS–NS binary mergers range from 0.4 to 400 year^{−1}, and such systems could be detectable to distances of several hundred Mpc (Abadie, the LIGO Scientific Collaboration & the Virgo Collaboration 2010; Aasi, the LIGO Scientific Collaboration & the Virgo Collaboration 2013). Similar rate estimates apply to NS-BH binaries. These numbers are, however, far more uncertain (by several orders of magnitude) since they rely on population synthesis alone (Abadie, the LIGO Scientific Collaboration & the Virgo Collaboration 2010). NS-BH binaries are detectable to much larger distances (> 1 Gpc, depending on the mass of the BH) thanks to their larger masses (which leads to a higher amplitude GW). Short-hard gamma-ray bursts (SGRBs) are believed to originate in the mergers of NS binaries (e.g., Fong & Berger 2013 and references therein), and could therefore provide GW standard sirens with EM counterparts (Dalal *et al.* 2006, hereafter D06). In addition, another potentially important standard siren is afforded by “macronovae” or “kilonovae” (e.g., Li & Paczyński 1998; Kulkarni 2005; Metzger *et al.* 2010; Roberts *et al.* 2011; Barnes & Kasen 2013; Kasen, Badnell & Barnes 2013), which are weak supernova-like transients with isotropic emission fueled by radioactive powered ejecta resulting from the mergers of NS–NS and NS–BH binaries.

The D06 analysis considered measurements using an advanced four-detector network that included an Australian detector (whose construction was until fairly recently under consideration). It also used a parameter estimation formalism based on a Gaussian approximation to the posterior likelihood function. This approximation is strictly correct only for “high” signal-to-noise ratio (SNR), although it is not clear what “high” means in this context (Cutler & Flanagan 1994; Vallisneri 2008). This is troublesome for ground-based GW detectors where most measurements are expected to be low SNR (near threshold). As a consequence, D06 *underestimates* the distance errors that we expect.

In Nissanke *et al.* (2010) (hereafter N10) we revisited the D06 analysis by following a Bayesian approach for estimating parameter errors instead of a Fisher matrix analysis (Finn 1992). We implemented a Metropolis-Hastings Markov Chain Monte-Carlo (MCMC) method to explore the posterior distribution of GW model parameters, in particular for deriving measurement errors in the luminosity distance. This was done for both NS–NS and NS–10 M_{\odot} BH binaries, using a careful selection procedure to decide which binaries to include in the analysis. N10 also used a more accurate inspiral waveform

than was used in D06, and considered various Northern and Southern Hemisphere ground-based detector networks. Specifically, in N10 we examined measurement accuracies at different network combinations of LIGO Hanford, LIGO Livingston, Virgo, KAGRA (formally known as the “Large-scale Cryogenic Gravitational-wave Telescope”)¹¹, and AIGO/LIGO Australia (Munch *et al.* 2011). We also considered how beaming of the SGRB, derived from observations using present or future γ -ray observatories, reduces measurement errors in the luminosity distance. In N10 we found that the distance to an individual NS–NS binary is measured to within a fractional error of roughly 20–60%, with 20–30% being representative for the majority of events in our detected distribution. If the orientation of the orbital plane of the NS–NS binary is assumed to be face-on (as might be expected for beamed SGRBs), we found that distance measurement errors improve by approximately a factor of two. If we instead assume that the EM counterparts are NS–10 M_{\odot} BH mergers, we found that the distribution of fractional distance errors ranges from 15–50%, with most events clustered near 15–25%. Assuming that the EM counterpart is a beamed SGRB reduces the measurement errors by a factor of two.

In what follows we update and refine the analysis of D06 and N10. This paper focuses on the implications such measurements will have when constraining cosmological parameters such as H_0 . Subtle and important differences exist between our current analysis and that used in N10. Primarily, we are interested here in H_0 constraints for the ensemble of GW-EM events, and not in individual distance measures for GW-EM event as in N10. In addition to collimated SGRBs, we also consider more speculative transients, such as macronovae or kilonovae, associated with NS binary mergers that emit isotropically in the optical or near infrared. For consistency with N10, we assume that the BHs in our NS–BH populations have masses of 10 M_{\odot} . We note, however, that recent numerical relativity simulations suggest that tidal disruption, and hence EM signatures, may only occur for NS–BH mergers with much smaller BH masses ($\sim 5 M_{\odot}$); see e.g., Taniguchi *et al.* (2007), Shibata & Taniguchi (2008), Shibata *et al.* (2009), Kyutoku *et al.* (2011), Foucart *et al.* (2011), Foucart (2012). In addition, we examine measurement accuracies for networks including LIGO India, an advanced interferometer whose construction is currently under consideration (Sathyaprakash 2012). Finally, in contrast to traditional standard candles such as Cepheid variables and Type Ia supernovae, we wish to emphasize that GW standard sirens are independent of the cosmological distance ladder. Compared with other recent standard siren studies using advanced GW interferometers (see e.g., Del Pozzo 2012; Taylor, Gair & Mandel 2012; Messenger & Read 2012), we consider the case where an EM observation of the NS binary inspiral is seen in conjunction with a GW measurement.

In the next section we summarize the principles underlying GW standard sirens. We then outline how we select our sample of binaries, and discuss the Bayesian method employed when estimating the luminosity distance for each source. We conclude by discussing future

⁹ <http://www.ligo.caltech.edu/advLIGO/>

¹⁰ <http://www.ego-gw.it/public/virgo/virgo.aspx>

¹¹ <http://gw.icrr.u-tokyo.ac.jp:8888/lcgt/>

constraints on H_0 , the results of which are critically dependent on the assumed source population’s characteristics and the specific advanced detector network.

2. STANDARD SIREN BINARIES

Many key observational methods employed in mapping out the expansion history of the universe rely on the luminosity distance-redshift relation:

$$D_L(z) = \frac{c(1+z)}{H_0\sqrt{\Omega_K}} \sinh \left[\sqrt{\Omega_K} \int_0^z \frac{H_0}{H(z')} dz' \right], \quad (1)$$

where the luminosity distance $D_L(z)$ is given as a redshift integral of the Hubble parameter $H(z)$, and the Hubble constant H_0 . For $z \gtrsim 1$, the evolution of $H(z)$ and $D_L(z)$ depends on cosmological parameters like Ω_m and w , through the Friedmann equations. However, for low redshifts $z \ll 1$, the distance-redshift relation is well described by $D_L(z) \approx cz/H_0$, independent of other cosmological parameters. This is why measurements of the distances to local sources, like Cepheids or GW standard sirens, can constrain the value of the Hubble constant.

The inspiral signal of the GWs, modeled accurately using the post-Newtonian (PN) approximation in general relativity, encodes geometrical and physical parameters of the source (see e.g., Blanchet 2006). The source parameters include: the binary’s luminosity distance D_L , its position on the sky \mathbf{n} , its redshifted chirp mass $\mathcal{M}_z = (1+z)m_1^{3/5}m_2^{3/5}/(m_1+m_2)^{1/5}$ where m_1 and m_2 denote the mass of each compact object in the binary, its redshifted reduced mass $\mu_z = (1+z)m_1m_2/(m_1+m_2)$, its orientation on the sky given by its inclination angle ι , where $\cos \iota = \mathbf{L} \cdot \mathbf{n}/|\mathbf{L}|$ and \mathbf{L} is the binary’s orbital angular momentum, and t_c and Φ_c , the time and GW phase at merger. A single detector a measures a linear combination of the two GW polarizations:

$$h_{a,\text{meas}}(\theta) = \mathbf{F}_+(\theta, \phi, \psi) \mathbf{h}_+ + \mathbf{F}_\times(\theta, \phi, \psi) \mathbf{h}_\times. \quad (2)$$

The colatitude θ and longitude ϕ describe the binary’s position on the sky \mathbf{n} . The polarization angle ψ sets the inclination of the components of the unit vector $\hat{\mathbf{L}}$ orthogonal to the unit vector $\hat{\mathbf{n}}$. The components of the vector θ are all the various parameters (masses, angles, distance, etc.) upon which this measured waveform depends. For the two GW polarizations h_+ and h_\times , we use the non-spinning restricted 3.5PN waveform in the frequency domain (indicated by the \tilde{h} notation):

$$\tilde{h}_+(f) = \sqrt{\frac{5}{96}} \frac{\pi^{-2/3} \mathcal{M}_z^{5/6}}{D_L} [1 + (\hat{\mathbf{L}} \cdot \hat{\mathbf{n}})^2] f^{-7/6} e^{i\Psi(f)}, \quad (3)$$

$$\tilde{h}_\times(f) = \sqrt{\frac{5}{96}} \frac{\pi^{-2/3} \mathcal{M}_z^{5/6}}{D_L} (\hat{\mathbf{L}} \cdot \hat{\mathbf{n}}) f^{-7/6} e^{i\Psi(f) - i\pi/2}, \quad (4)$$

which relies on the “stationary phase” approximation (Finn & Chernoff 1993), where the GW frequency f varies slowly over a single wave period. The GW phase in the frequency domain Ψ is computed to 3.5 PN order, where $\Psi(f)$ is given by:

$$\Psi(f) = 2\pi f t_c - \Phi_c - \frac{\pi}{4} + \frac{3}{128} (\pi \mathcal{M}_z f)^{-5/3} \times \left[1 + \frac{20}{9} \left(\frac{743}{336} + \frac{11}{4} \eta \right) (\pi M_z f)^{2/3} \right.$$

$$\left. -16\pi(\pi M_z f) + 10 \left(\frac{3058673}{1016064} + \frac{5429}{1008} \eta \right. \right. \\ \left. \left. + \frac{617}{144} \eta^2 \right) (\pi M_z f)^{4/3} + \pi \left(\frac{38645}{756} - \frac{65}{9} \eta \right) \right. \\ \left. \times \left[1 + (\pi M_z f)^{5/3} \ln \left(\frac{f}{f_0} \right) \right] \right. \\ \left. + \left[\frac{11583231236531}{4694215680} - \frac{640}{3} \pi^2 - \frac{6848}{21} \gamma \right] (\pi M_z f)^2 \right. \\ \left. \left[\left(-\frac{15335597827}{3048192} + \frac{2255}{12} \pi^2 - \frac{47324}{63} - \frac{7948}{9} \right) \eta \right. \right. \\ \left. \left. + \frac{76055}{1728} \eta^2 - \frac{127825}{1296} \eta^3 \right] (\pi M_z f)^2 \right. \\ \left. + \pi \left[\frac{77096675}{254016} + \frac{378515}{1512} \eta - \frac{74045}{756} \eta^2 \right] \right. \\ \left. (\pi M_z f)^{7/3} \right], \quad (5)$$

where $M_z = (1+z)(m_1+m_2)$ is the binary’s redshifted total mass, $\eta = \mu_z/M_z$ is defined as the binary’s symmetric mass parameter, γ is Euler’s constant, and f_0 is a constant frequency scale (Blanchet 2006). Central to the results of this paper and N10, key geometrical source parameters, such as D_L and $\cos \iota$, appear in the amplitude of each GW polarization $\tilde{h}_\times(f)$ and $\tilde{h}_+(f)$. Therefore, measurement errors in D_L and $\cos \iota$ depend on the extent of the degeneracy between these and other parameters appearing only in the amplitude. We hence wish to assess how well we can disentangle each polarization from the measured GW strain at a detector.

Beyond the redshifting of masses (which is a simple consequence of the cosmological redshift of all timescales), this waveform model does not encode any information about source redshift. To investigate the D_L - z relationship, in this work we require an independent measure of the source’s z by observing an EM counterpart. Other methods of obtaining the source’s redshift include using statistical arguments regarding the underlying NS binary merger distribution (e.g., Taylor, Gair & Mandel 2012), or adding information about the NSs’ (non-redshifted) tidal deformation in the GW phase (e.g., Messenger & Read 2012). Del Pozzo (2012) uses galaxy catalogs to infer probabilistically sources’ redshifts. In contrast, an EM counterpart detected with a GW measurement may also advantageously indicate the source’s sky position. As was shown in N10, localizing the binary with independent EM observations reduces measurement errors in parameters D_L and $\cos \iota$ by breaking correlations with other parameters, and by reducing the dimensionality of the parameter space. An EM counterpart may also bring information about the time of merger for the binary, which will increase the detection range of a coherent network by a factor of ~ 1.2 (e.g., Kelley, Mandel & Ramirez-Ruiz 2013; Dietz *et al.* 2013).

3. METHOD

This section summarizes the methodology used to derive H_0 measurements for an ensemble of NS-NS or NS-BH binary mergers. We first outline the schema of our method. Based on Sections 3 and 4 of N10, we then describe technical aspects of simulating anticipated dis-

tance measurements.

3.1. Schema of our method

We detail below how we construct the posterior probability density function (PDF) in H_0 for a set of detected GW-EM standard siren measurements. Deriving H_0 constraints for ensembles of NS binary mergers requires particular care, as we expect that the majority of events will be detected at low SNR. Consequently, PDFs in H_0 for individual events will depend significantly on our prior knowledge of the events' parameter distributions. In this study, how we select for GW-EM events determines our choice in specific priors.

We envision a scenario in which we have detected a total of m GW-EM events. Each event has both a GW measurement of distance, $D_{L,i}$, and an EM redshift, z_i , where the subscript i represents a particular binary and runs from $1 \dots m$. When combined these produce a value for H_0 [see Eq. (1)]. We assume a model that is described by: i) the event's underlying redshift distribution denoted by X , ii) each source's *true* redshift \hat{z}_i , and iii) the vector set of source parameters θ_i^R for a single measured GW binary. As shown in Eq. (1), the luminosity distance for a specific GW event depends on both H_0 and \hat{z} , and thus, we do *not* include $D_{L,i}$ in θ_i^R . The set θ^R differs from the set θ , which includes the parameter D_L and was used in N10. In N10 we were interested in luminosity distance measurements for individual events and not for ensemble GW-EM standard sirens as in this work.

The data matrix $\{\mathbf{s}_i, z_i\}$ comprises the measured GW time streams \mathbf{s}_i , and the set of *observed* EM redshifts z_i for a set of m binaries. If we assume that our model parameters are independent of one another, the prior $p_{\text{prior}}(H_0, X, \hat{z}_i, \theta_i^R)$ for m detected GW-EM coincident events is given by:

$$p_{\text{prior}}(H_0, X, \hat{z}_i, \theta_i^R) = \mathcal{A} p_0(H_0) p_0(X) \times \prod_{i=1}^m p_0(\hat{z}_i|X) p_0(\theta_i^R), \quad (6)$$

where $p_0(H_0)$, $p_0(X)$, and $p_0(\theta_i^R)$ are the individual priors on H_0 , X , and θ_i^R . The quantity $p_0(\hat{z}_i|X)$ is the prior distribution on a GW-EM event's true redshift given the underlying distribution X , and \mathcal{A} is a normalization constant. We introduce the likelihood function \mathcal{L} , which measures the relative conditional probability of observing the sources' redshifts z_i (via EM measurements), and a particular set of data \mathbf{s}_i (via GWs) given the source's parameters θ_i^R . It assumes the form:

$$\mathcal{L}(\{\mathbf{s}_i, z_i\}|H_0, X, \hat{z}_i, \theta_i^R) = \prod_{i=1}^m \mathcal{L}(\mathbf{s}_i|H_0, z_i, \theta_i^R) P(z_i|\hat{z}_i), \quad (7)$$

where the likelihood function for a single GW event is

$$\mathcal{L}(\mathbf{s}_i|H_0, z_i, \theta_i^R) = e^{-(h_a(\theta) - s_a | h_a(\theta) - s_a)/2}. \quad (8)$$

The inner product $(g|h)$ describes the noise-weighted cross correlation of $g(t)$ and $h(t)$ on the vector space of

signals, and is defined as:

$$(g|h) = 2 \int_0^\infty df \frac{\tilde{g}^*(f) \tilde{h}(f) + \tilde{g}(f) \tilde{h}^*(f)}{S_n(f)}, \quad (9)$$

where $S_n(f)$ denotes the instrument's power spectral density. The Fourier transform $\tilde{h}(f)$ of $h(t)$ is defined as:

$$\tilde{h}(f) \equiv \int_{-\infty}^\infty e^{2\pi i f t} h(t) dt. \quad (10)$$

An important element of our analysis is that we express the *joint posterior* PDF in H_0 given m observed GW-EM events as:

$$p_{\text{joint}}(H_0|\{\mathbf{s}_i, z_i\}) \propto p_{\text{prior}}(H_0, X, \hat{z}_i, \theta_i^R) \times \mathcal{L}(\{\mathbf{s}_i, z_i\}|H_0, X, \hat{z}_i, \theta_i^R), \\ = \mathcal{N} p_0(H_0) \int dX p_0(X) \left\{ \prod_{i=1}^m \int d\hat{z}_i p_0(\hat{z}_i|X) P(z_i|\hat{z}_i) \times \left[\int d\theta_i^R p_0(\theta_i^R) \times \mathcal{L}(\mathbf{s}_i|H_0, X, z_i, \theta_i^R) \right] \right\}, \quad (11)$$

where \mathcal{N} is a normalization constant and we substitute Eqs. (6) and (7) for the model's prior and likelihood functions respectively. In the event where we have the precise redshift measurement of binary i 's EM counterpart [i.e., $p(z_i|\hat{z}_i) = \delta(z_i - \hat{z}_i)$], Eq. (11) then reduces to:

$$p_{\text{joint}}(H_0|\{\mathbf{s}_i, z_i\}) = \mathcal{N} p_0(H_0) \int dX p_0(X) \left\{ \prod_{i=1}^m p_0(z_i|X) \times \left[\int d\theta_i^R p_0(\theta_i^R) \times \mathcal{L}(\mathbf{s}_i|H_0, X, z_i, \theta_i^R) \right] \right\} \\ = \mathcal{N} p_0(H_0) \left[\int dX p_0(X) \prod_{i=1}^m p_0(z_i|X) \right] \times \prod_{i=1}^m \left\{ \int d\theta_i^R p_0(\theta_i^R) \times \mathcal{L}(\mathbf{s}_i|H_0, X, z_i, \theta_i^R) \right\} \\ = \mathcal{N}' p_0(H_0) \times \prod_{i=1}^m \left\{ \int d\theta_i^R p_0(\theta_i^R) \times \mathcal{L}(\mathbf{s}_i|H_0, X, z_i, \theta_i^R) \right\}. \quad (12)$$

The normalization constant \mathcal{N}' absorbs the $[\dots]$ part appearing in the previous line, which is independent of H_0 . We assume a uniform prior in H_0 such that $p_0(H_0) = \text{constant}$. It is worth noting that our formalism could be generalized to include the most precise current estimates of H_0 . We do not do this here, although we certainly

imagine that this would be done when one does an analysis of this sort with actual GW detections.

Since we take p_0 to be constant, we need only compute the $\{\dots\}$ term in the last part of Eq. (12), where θ_i^R does not include D_L . Outlined below, our work relies on computing the key term:

$$p_0(\theta_i^R) \mathcal{L}(\mathbf{s}_i|H_0, X, z_i, \theta_i^R) \quad (13)$$

for each GW-EM event. This contrasts with the methods used in N10, where we instead computed the term $p_0(\theta_i) \mathcal{L}(\mathbf{s}_i|\theta_i)$ for each binary, where θ included D_L .

3.2. Summary of MCMC approach used

For each GW-EM event we explicitly map out the term $p_0(\theta_i^R) \mathcal{L}_{\text{TOT}}(\mathbf{s}_i|X, z_i, \theta_i)$ using MCMC methods (see N10 and Nissanke *et al.* 2011 for details). The vector set θ now includes D_L because of the one-to-one mapping between D_L and H_0 . The quantity $\mathcal{L}_{\text{TOT}}(\mathbf{s}_i|X, z_i, \theta_i)$ is the likelihood function for an entire network. We assume that the instrument noise \mathbf{n} is Gaussian, independent, and uncorrelated at each detector site. Therefore, the network likelihood function is the product of the individual likelihoods at each detector. We generate the signal \mathbf{s}_a at each detector a such that it comprises the predicted GW signal $\mathbf{h}_a(\hat{\theta})$, which depends on the set of true source parameters $\hat{\theta}$, and the instrument noise \mathbf{n}_a . In our study we use the projected advanced LIGO sensitivity curve for $S_n(f)$ shown in N10 and denoted “Zero-Detuned, High-Power” in Harry & the LIGO Scientific Collaboration (2010) for all our GW interferometers.

We generate predicted templates \mathbf{h}_a (and hence also the measured signals \mathbf{s}_a) using the PN description of the binaries as the bodies inspiral about one another prior to their merger. Specifically, we use the restricted 3.5PN waveform in the frequency domain, where the GW frequency evolves with a characteristic chirp [see Eqns. (4)–(6)]. We note that the largest contribution to the signal accumulates from the inspiral (and not the subsequent merger and ringdown parts of the waveform) for NS binaries in the frequency band of ground based interferometers (Flanagan & Hughes 1998). When the sky position \mathbf{n} is assumed known from its EM counterpart observation, the GW strain at each detector, $\mathbf{h}_a(t; \hat{\theta})$, is described using seven parameters, θ : the two redshifted mass parameters (\mathcal{M}_z and μ_z), two orientation angles (Ψ and $\cos \iota$), the GW merger’s time and phase (t_c and Φ_c), and the binary’s luminosity distance (D_L). Apart from excluding D_L , the six parameters in the reduced vector set θ^R are identical to those in θ .

We use the MCMC algorithm discussed in Section 3.3 of N10 to explore the likelihood function. For binaries with an underlying population with isotropic orientation, we take prior distributions in the sources’ parameters to be flat over the region of sample space that corresponds to our threshold SNR (described below). For the subset of beamed binaries, we assume a uniform prior on the SGRB’s beaming angle distribution in the range of $|\cos \iota| > 0.94$, which corresponds to a beamed population with an opening jet angle of approximately 20° (e.g., Burrows *et al.* 2006; Soderberg *et al.* 2006; Fong *et al.* 2012). We choose the prior such that it is fully consistent with how we select our subset of beamed SGRBs.

3.3. Binary Selection

We follow the approach of N10 in generating a sample of detectable GW-EM events. Having assumed a constant comoving density of GW-EM events in a Λ CDM universe (Komatsu *et al.* 2009), we distribute 10^6 binaries uniformly in volume with random sky positions and orientations to redshift $z = 1$ ($D_L \simeq 6.6$ Gpc).

By computing the expected network SNR (the root-sum-square of the expected SNRs at each detector) for each binary and comparing it to a threshold network SNR, we construct a *detected* sample of binary events for every network under consideration. Assuming prior knowledge of merger time and source position allows us to set the threshold for the network to $\text{SNR} = 7.5$, a value lower than that used in the absence of an EM counterpart (see D06 and N10). Figure 2 in N10 shows how the detectable GW-EM events for each detector network increases as the number of detectors in a network increases. Notice that N10 included an advanced detector in Australia and not LIGO India as in this work (the coordinates assumed for LIGO India are given in Nissanke, Kasliwal & Georgieva 2013). The term “total detectable binaries” refers to binaries which are detectable by a network of all five detectors — both LIGO sites, Virgo, LIGO India, and KAGRA.

Finally we obtain our subsample of beamed SGRBs from our original sample of total detected GW-EM binaries by assuming that the SGRB has a uniform beaming angle distribution of $|\cos \iota| > 0.94$.

4. RESULTS AND DISCUSSION

We now present our results for H_0 constraints using GW standard sirens observed by advanced ground-based GW detector networks. As discussed in Sec. 2, we are interested in the joint PDF of H_0 given an ensemble of GW-EM observations.

Figure 1 shows the normalized joint posterior PDFs in H_0 , indicated by the thick blue line, for a sample of 15 isotropically oriented NS-NS binaries observed with the baseline LIGO-Virgo network. The thin lines in Figure 1 represent each individual binary’s measurement of H_0 . We note that each binary gives a relatively poor constraint on H_0 with 68% confidence level (c.l.) fractional errors of ~ 30 –50%. The likelihood formalism results in the joint posterior PDFs in H_0 for an ensemble of 15 mergers detected by LIGO-Virgo network being peaked around our assumed true value of 70.5 km/s/Mpc with a standard deviation of 5 km/s/Mpc. This result would be competitive with current H_0 constraints using either the cosmological distance ladder (e.g., see Freedman *et al.* 2012, Riess *et al.* 2009a, Riess *et al.* 2009b) or VLBI water maser measurements (see e.g., Reid *et al.* 2009; Braatz *et al.* 2010; Kuo *et al.* 2011; Reid *et al.* 2013).

Table 1 presents the errors (68% c.l.) on H_0 as a function of the number of binaries detectable by a particular network. We randomly select 30 NS-NS and 30 NS-BH mergers detected in GWs using a five detector network. The actual number of detectable binaries is a function of the detector network, on whether the EM counterpart is collimated (as we expect in the case of SGRBs), and on whether the progenitor model is a NS-NS or NS-BH binary (N10, Chen & Holz 2012). Specifically, Table 1 shows the measurement errors in H_0 for samples

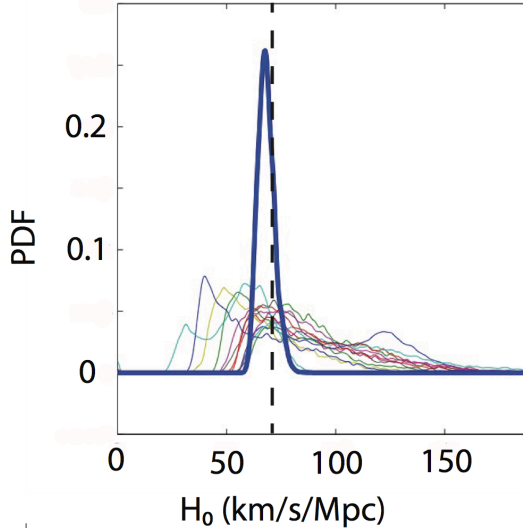


FIG. 1.— The joint posterior PDF in H_0 for a sample of 15 isotropically-oriented NS-NS binaries observed using a three detector network (LIGO Livingston, LIGO Hanford, Virgo). The light coloured lines mark the normalized posterior PDF for H_0 for each event, whereas the thicker blue line denotes the joint posterior PDF in H_0 given all the observed events. The vertical dashed black line denotes the value of H_0 of 70.5 km/s/Mpc used in generating the simulations. As the number of detections increases, the joint posterior PDF gets progressively narrower, and its center comes closer to the true value of H_0 .

of unbeamed and beamed NS-NS or NS-BH binaries using different detector networks. The percentage errors are quoted as the fraction of measured standard deviations over an assumed true value ($H_0 = 70.5$ km/s/Mpc). Such a measurement corresponds to a range of observation times because of the wide range of uncertainties in NS binary merger rates. The general trends seen in Table 1 can be summarized as:

- As expected, the errors in H_0 decrease with an increase in the number of GW detectors in a network. Table 1 shows that a five detector network will result in an improvement of up to a factor of 2 compared to a three detector network. Such a feature is a consequence of the increase in the *detected* number of binaries, rather than due to the decrease in measurement error in D_L for each individual event (see discussion in N10). Due to differences in the instruments' antenna response functions, the addition of LIGO India has a greater impact than that of KAGRA.
- The errors in H_0 reduce by a factor from two to five when the EM counterpart is assumed to be beamed. In the case of beamed NS binary mergers whose PDFs are more Gaussian in shape, we find that the error in H_0 decreases as $1/\sqrt{N}$, where N is the number of GW-EM events detected. We expect this trend in the joint PDF of H_0 as we fix the inclination angle of each binary in the ensemble, since individual H_0 constraints are Gaussian in distribution due to the absence of the $D_L \cos i$ degeneracy.

Fig. 2 shows the 68% c.l. measurement error in H_0 as a function of the number of GW-EM detectable NS binary merger events. We assume that our detectable sample

comprises 26 GW-EM binary mergers observed with a LIGO-Virgo network; we expect that the errors in H_0 will decrease with $1/\sqrt{N}$ in the limit of large N , where N is the number of detectable GW-EM events. We compute the posterior PDF in H_0 for each NS-NS binary merger in our sample averaged over 100 noise realizations. The solid bars indicate the measurement error in H_0 for the *joint* PDF of some i binary mergers; at low i , we select the i -th merger with the mean value in the H_0 error of the remaining $(26 - (i - 1))$ detectable GW-EM events. By doing so, we minimize the impact that arbitrary ordering for small i GW-EM events will have on the convergence of measurement errors in H_0 . For an identically-ordered ensemble of NS-NS mergers, the dashed line indicates the measurement error in H_0 derived assuming Gaussian errors for each GW-EM independent merger. In the limit of large i events, the difference in H_0 error constraints decreases between the two methods. Furthermore, for low i events in particular, we find that the non-Gaussian shapes of the individual H_0 distributions improve the combined H_0 distribution. For example and as discussed in N10, after observing 15 NS-NS mergers in GWs and EM, we find that H_0 may be measured to within 5% using the combined posterior PDF method (or to within 8% assuming Gaussian posterior PDFs for each individual event). Without an EM counterpart and based solely on statistical cross-correlations of GW sky errors with wide-field galaxy surveys, Del Pozzo (2012) finds a 14% H_0 measurement error (with a 95% confidence interval) using ten GW merger events with a LIGO-Virgo network (and assuming a SNR ~ 15).

We now explore how the number of detectable GW-EM NS binary merger events corresponds to an observable time window. From Abadie, the LIGO Scientific Collaboration & the Virgo Collaboration (2010), we use the mean NS-NS merger rate of $1 \text{ Mpc}^{-3} \text{ Myr}^{-1}$. We expect 15 (30) isotropically-oriented NS-NS mergers to be detectable in GWs over a \sim three month period using a three (five) GW detector network and an EM precursor trigger (Nissanke, Kasliwal & Georgieva 2013). If we instead consider beamed NS binary mergers and use the SGRB rate of $10 \text{ Gpc}^{-3} \text{ yr}^{-1}$, we expect ~ 30 GW-SGRB events per year (Berger 2011; Chen & Holz 2012; Enrico Petrillo, Dietz & Cavaglia 2013).

In the case of isotropically-oriented NS-10 M_\odot BH mergers, we use a merger rate of $0.03 \text{ Mpc}^{-3} \text{ Myr}^{-1}$ (Abadie, the LIGO Scientific Collaboration & the Virgo Collaboration 2010). We then expect 15 (30) GW-detectable events in GWs over a six month period (we scale the results given in Table 1 of Nissanke, Kasliwal & Georgieva 2013 by a factor $\mathcal{M}_c^{5/6}$ to account for the difference between the NS-10 M_\odot BH and the NS-5 M_\odot BH mergers used there and here respectively). Due to an absence of observed systems, we emphasize that NS-BH merger rates based on population synthesis results vary by several orders of magnitude. In the case of beamed NS-BH mergers, we use the SGRB rate of $10 \text{ Gpc}^{-3} \text{ yr}^{-1}$ and find 1 GW-SGRB event per year (e.g., Chen & Holz 2012; Enrico Petrillo, Dietz & Cavaglia 2013; Kelley, Mandel & Ramirez-Ruiz 2013; Dietz *et al.* 2013).

Although it is clear that of order 20–30 events are needed to reach percent level accuracy in determining H_0 , it is unclear how long this will take given the range

TABLE 1

MEASUREMENT ERRORS IN H_0 FOR A SAMPLE OF GW-EM EVENTS. RESULTS ARE PRESENTED FOR UNBEAMED AND BEAMED SOURCES, FOR BOTH NS-NS AND NS-BH MERGERS, AND FOR A RANGE OF DETECTOR NETWORKS. THE % VALUES ARE THE 68% C.L. FRACTIONAL ERRORS, AND THE NUMBER OF BINARIES DETECTED BY EACH NETWORK IS GIVEN IN PARENTHESES.

Network	LIGO+Virgo (LLV)	LLV+LIGO India	LLV+KAGRA	LLV+LIGO India+KAGRA
NS-NS Isotropic	5.0% (15)	3.3% (20)	3.2% (20)	2.1% (30)
NS-NS Beamed	1.1% (19)	1.0% (26)	1.0% (25)	0.9% (30)
NS-BH Isotropic	4.9% (16)	3.5% (21)	3.6% (19)	2.0% (30)
NS-BH Beamed	1.2% (18)	1.0% (25)	1.1% (24)	0.9% (30)

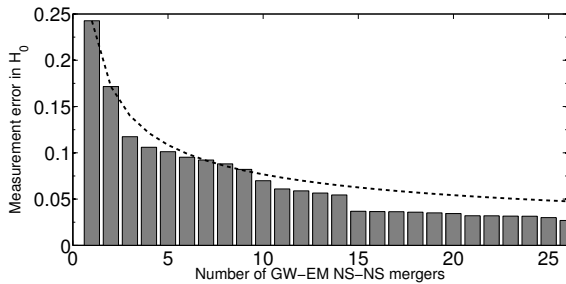


FIG. 2.— H_0 measurement error as a function of the number of multi-messenger (GW+EM) NS-NS merger events observed by a LIGO-Virgo network. The solid bars indicate the 68% c.l. measurement error in H_0 for the *joint* PDF of the independent binary mergers; the dashed line shows the 68% c.l. measurement error in H_0 derived assuming Gaussian errors for each GW-EM merger. When specifying the particular order of events shown, we choose the GW-EM merger in the remaining ensemble with the mean measurement error in H_0 .

of uncertainty in binary merger rates. Current estimates suggest that the median timescale to achieve this number of events is likely about one year, but could be as short as a few months, or as long as a decade.

5. IMPLICATIONS FOR COSMOLOGY

Assuming GR accurately describes the inspiral dynamics and GW emission, GW standard sirens should provide a measure of H_0 based on *absolutely-calibrated* GW distances that are independent of the cosmological distance ladder. Given that we anticipate a network of advanced GW interferometers reaching their design sensitivity within the next decade, this physics-based technique could play a large role in precision determination of the Hubble constant, especially in conjunction with other approaches (see Suyu *et al.* 2012 and references therein).

In this work, by envisioning a range of scenarios using different networks of GW detectors and different populations of NS binary progenitors, we show that ensembles of GW standard sirens have the power to constrain H_0 to an accuracy of $\sim 1\%$. We have assumed joint GW and EM observations of the NS binary merger; other works, for instance Taylor, Gair & Mandel (2012), Del Pozzo (2012) and Messenger & Read (2012), examine H_0 constraints using solely GW observations, and are based on statistical arguments or galaxy catalogs to infer the mergers' redshifts. We emphasize that an individual standard siren may only constrain H_0 to a precision ranging from 5 to 50%. We have shown that the error in H_0 depends critically on *the number of GW-EM mergers observed*, which in turn depends on the NS binary progenitor, on whether the NS binary is face-on (due to GRB beaming),

and on the number and sensitivity of GW interferometers in a network. We find that the critical limitation when projecting the timescale for this measurement (once the GW detectors are operational) is the few orders of magnitude uncertainty in NS binary merger rates, independent of GW detections. Using mean NS merger rates derived from population synthesis or the observed Galactic binary pulsar distribution, we estimate that percent-level measurements of H_0 are possible within ~ 1 year of observation, or may take as long as a decade for pessimistic event rates.

For flat cosmologies, a measurement of H_0 at the percent level, when combined with precision CMB measurements of the absolute distance to the last scattering surface, would constrain the dark energy equation of state parameter w to $\sim 10\%$ (D06). The power of such a result (e.g., to falsify the cosmological constant model for dark energy) depends critically on understanding the systematic errors associated with the measurement of H_0 . It is for this reason that GW standard sirens may have an important role to play in constraining cosmology in the near future.

6. ACKNOWLEDGEMENTS

We thank Curt Cutler, Phil Marshall, and Michele Valisneri for very useful discussions on selection effects and biases. We thank Vicky Scowcroft for discussion on H_0 measurements, Edo Berger, Josh Bloom and Brian Metzger for discussions on GW-GRB measurements, and Francois Foucart for discussion on the status of numerical relativity simulations. Some of the simulations were performed using the Sunnyvale cluster at Canadian Institute for Theoretical Astrophysics (CITA), which is funded by NSERC and CIAR. Part of this work was performed at the Jet Propulsion Laboratory, California Institute of Technology, under contract with the National Aeronautics and Space Administration. SMN is supported by the David & Lucile Packard Foundation. ND is supported by NASA under grants NNX12AD02G and NNX12AC99G, and by a Sloan Research Fellowship from the Alfred P. Sloan Foundation. DEH acknowledges support from National Science Foundation CAREER grant PHY-1151836. SAH is supported by NSF Grant PHY-1068720. SAH also gratefully acknowledges fellowship support by the John Simon Guggenheim Memorial Foundation, and sabbatical support from CITA and the Perimeter Institute for Theoretical Physics. CH is supported by the Simons Foundation, the David & Lucile Packard Foundation, and the US Department of Energy (award de-sc0006624).

REFERENCES

- Aasi, J., the LIGO Scientific Collaboration, and the Virgo Collaboration 2013, ArXiv e-prints, 1304.0670.
- Abadie, J., the LIGO Scientific Collaboration, and the Virgo Collaboration 2010, *Classical and Quantum Gravity*, 27(17), 173001, 1003.2480.
- Barnes, J. and Kasen, D. 2013, ArXiv e-prints, 1303.5787.
- Berger, E. 2011, *New Ast. Rev.*, 55, 1, 1005.1068.
- Blanchet, L. 2006, *Living Reviews in Relativity*, 9, 4.
- Bloom, J. S. *et al.* 2009, ArXiv e-prints, 0902.1527.
- Braatz, J. A., Reid, M. J., Humphreys, E. M. L., Henkel, C., Condon, J. J., and Lo, K. Y. 2010, *ApJ*, 718, 657, 1005.1955.
- Burrows, D. N. *et al.* 2006, *ApJ*, 653, 468, arXiv:astro-ph/0604320.
- Chen, H.-Y. and Holz, D. E. 2012, ArXiv e-prints, 1206.0703.
- Cutler, C. and Flanagan, É. E. 1994, *Phys. Rev. D*, 49, 2658, arXiv:gr-qc/9402014. referred to in the text as CF94.
- Dalal, N., Holz, D. E., Hughes, S. A., and Jain, B. 2006, *Phys. Rev. D*, 74(6), 063006, arXiv:astro-ph/0601275. referred to in the text as D06.
- Del Pozzo, W. 2012, *Phys. Rev. D*, 86(4), 043011, 1108.1317.
- Dietz, A., Fotopoulos, N., Singer, L., and Cutler, C. 2013, *Phys. Rev. D*, 87(6), 064033, 1210.3095.
- Enrico Petrillo, C., Dietz, A., and Cavaglià, M. 2013, *ApJ*, 767, 140, 1202.0804.
- Finn, L. S. 1992, *Phys. Rev. D*, 46, 5236, arXiv:gr-qc/9209010.
- Finn, L. S. and Chernoff, D. F. 1993, *Phys. Rev. D*, 47, 2198, arXiv:gr-qc/9301003.
- Flanagan, É. E. and Hughes, S. A. 1998, *Phys. Rev. D*, 57, 4535, arXiv:gr-qc/9701039.
- Fong, W. *et al.* 2012, *ApJ*, 756, 189, 1204.5475.
- Fong, W.-f. and Berger, E. 2013, ArXiv e-prints, 1307.0819.
- Foucart, F. 2012, *Phys. Rev. D*, 86(12), 124007, 1207.6304.
- Foucart, F., Duez, M. D., Kidder, L. E., and Teukolsky, S. A. 2011, *Phys. Rev. D*, 83(2), 024005, 1007.4203.
- Freedman, W. L., Madore, B. F., Scowcroft, V., Burns, C., Monson, A., Persson, S. E., Seibert, M., and Rigby, J. 2012, *ApJ*, 758, 24, 1208.3281.
- Harry, G. M. and the LIGO Scientific Collaboration 2010, *Classical and Quantum Gravity*, 27(8), 084006.
- Hu, W. 2005, in *Observing Dark Energy*, ed. S. C. Wolff and T. R. Lauer, volume 339 of *Astronomical Society of the Pacific Conference Series*, 215. arXiv:astro-ph/0407158.
- Kasen, D., Badnell, N. R., and Barnes, J. 2013, ArXiv e-prints, 1303.5788.
- Kelley, L. Z., Mandel, I., and Ramirez-Ruiz, E. 2013, *Phys. Rev. D*, 87(12), 123004, 1209.3027.
- Komatsu, E. *et al.* 2009, *ApJS*, 180, 330, 0803.0547.
- Kulkarni, S. and Kasliwal, M. M. 2009, in *Astrophysics with All-Sky X-Ray Observations*, ed. N. Kawai, T. Mihara, M. Kohama, and M. Suzuki, 312. 0903.0218.
- Kulkarni, S. R. 2005, ArXiv Astrophysics e-prints, arXiv:astro-ph/0510256.
- Kuo, C. Y. *et al.* 2011, *ApJ*, 727, 20, 1008.2146.
- Kyutoku, K., Okawa, H., Shibata, M., and Taniguchi, K. 2011, *Phys. Rev. D*, 84(6), 064018, 1108.1189.
- Li, L.-X. and Paczyński, B. 1998, *ApJ*, 507, L59, arXiv:astro-ph/9807272.
- Messenger, C. and Read, J. 2012, *Physical Review Letters*, 108(9), 091101, 1107.5725.
- Metzger, B. D. *et al.* 2010, *MNRAS*, 406, 2650, 1001.5029.
- Munch, J. *et al.* 2011. <https://dcc.ligo.org/cgi-bin/DocDB/ShowDocument?docid=11666>.
- Nissanke, S., Holz, D. E., Hughes, S. A., Dalal, N., and Sievers, J. L. 2010, *ApJ*, 725, 496, 0904.1017. referred to in the text as N10.
- Nissanke, S., Kasliwal, M., and Georgieva, A. 2013, *ApJ*, 767, 124, 1210.6362.
- Nissanke, S., Sievers, J., Dalal, N., and Holz, D. 2011, *ApJ*, 739, 99, 1105.3184.
- Phinney, E. S. 2009, ArXiv e-prints, 0903.0098.
- Planck Collaboration *et al.* 2013, ArXiv e-prints, 1303.5076.
- Reid, M. J., Braatz, J. A., Condon, J. J., Greenhill, L. J., Henkel, C., and Lo, K. Y. 2009, *ApJ*, 695, 287, 0811.4345.
- Reid, M. J., Braatz, J. A., Condon, J. J., Lo, K. Y., Kuo, C. Y., Impellizzeri, C. M. V., and Henkel, C. 2013, *ApJ*, 767, 154, 1207.7292.
- Riess, A. G. *et al.* 2011a, *ApJ*, 732, 129.
- Riess, A. G. *et al.* 2011b, *ApJ*, 730, 119, 1103.2976.
- Riess, A. G. *et al.* 2009a, *ApJ*, 699, 539, 0905.0695.
- Riess, A. G. *et al.* 2009b, *ApJS*, 183, 109, 0905.0697.
- Roberts, L. F., Kasen, D., Lee, W. H., and Ramirez-Ruiz, E. 2011, *ApJ*, 736, L21, 1104.5504.
- Sathyaprakash, B. *et al.* 2012. <https://dcc.ligo.org/cgi-bin/DocDB/ShowDocument?docid=91470>.
- Schutz, B. F. 1986, *Nature*, 323, 310.
- Shibata, M., Kyutoku, K., Yamamoto, T., and Taniguchi, K. 2009, *Phys. Rev. D*, 79(4), 044030, 0902.0416.
- Shibata, M. and Taniguchi, K. 2008, *Phys. Rev. D*, 77(8), 084015, 0711.1410.
- Soderberg, A. M. *et al.* 2006, *ApJ*, 650, 261, arXiv:astro-ph/0601455.
- Suyu, S. H. *et al.* 2012, ArXiv e-prints, 1202.4459.
- Taniguchi, K., Baumgarte, T. W., Faber, J. A., and Shapiro, S. L. 2007, *Phys. Rev. D*, 75(8), 084005, arXiv:gr-qc/0701110.
- Taylor, S. R., Gair, J. R., and Mandel, I. 2012, *Phys. Rev. D*, 85(2), 023535, 1108.5161.
- Vallisneri, M. 2008, *Phys. Rev. D*, 77(4), 042001, arXiv:gr-qc/0703086.
- Weinberg, D. H., Mortonson, M. J., Eisenstein, D. J., Hirata, C., Riess, A. G., and Rozo, E. 2012, ArXiv e-prints, 1201.2434.